Polyelectrolyte mannan from diatoms reshapes sunlit ocean microbiome

J. Krull[1,2,6], C.J. Crawford[4], C. Sidhu[3], V. Solanki[3], M. Bligh[3], L. Rößler[2,3], R.K. Singh[4], G. Huang[2,3], C.S. Robb[2,3], H. Teeling[3], P.H. Seeberger[4], T. Schweder[5,6], J-H. Hehemann[1,2,3,6]*

[1] Department of Biology and Chemistry, University of Bremen, Leobener Straße 2, Germany

[2] MARUM-Center for Marine Environmental Sciences, Leobener Straße 2, University of Bremen, Germany

[3] Max Planck Institute for Marine Microbiology, Celsiusstraße 1, 28359, Bremen, Germany

[4] Max Planck Institute of Colloids and Interfaces, Am Mühlenberg 1, 14476, Potsdam, Germany

[5] Pharmaceutical Biotechnology, Institute of Pharmacy, University of Greifswald, Felix-Hausdorff-Straße 3, 17487 Greifswald, Germany

[6] Institute of Marine Biotechnology, Walther-Rathenau-Straße 49a, 17489 Greifswald, Germany

*jhhehemann@marum.de

Abstract

Algae catalyze half of the global solar powered reduction of carbon dioxide to organic molecules. While this organic synthesis shapes genomes of heterotrophic microbiota globally, many corresponding structures remain elusive. We show that diatoms release a mannan polyelectrolyte selecting for bacteria with a specifically adapted enzymatic cascade. NMR spectroscopy, chromatography, automated glycan assembly and enzymatic dissection resolved the structure of a C6 sulfated α-1,3-mannan with exceptional simplicity for a sulfated polysaccharide from algae. Biochemical, physiological and structural analyses demonstrated that some bacteria can hydrolyze this mannan with a cascade of just four enzymes. Circumnavigation metagenome data revealed corresponding genes in Atlantic, Pacific, Southern and Indian Ocean surface waters. We show that this sulfated mannan may exert substantial selection pressure on marine microbiota around the globe.

Main

Do phototrophs or heterotrophs control the balance between capture and release of carbon dioxide that influences the Earth heat capacity? Phototrophic organisms including plants, algae and cyanobacteria chemically reduce carbon dioxide to organic molecules at an estimated rate of 380 Gt year^{-1} (*1*). In the ocean, released photosynthesized organic molecules can store carbon in sediments, in dissolved form, in particles, or in living organisms until they are oxidized back to carbon dioxide, a process largely catalyzed by heterotrophic bacteria. This ability is due to the short generation times of bacteria in combination with extensive gene birth, duplication, loss and transfer (*2*) providing the many different types of enzymes required to recognize and oxidize organic molecules (*3*). For example, carbohydrate polymers, or glycans, which represent the most diverse macromolecules in nature (*4*) are primarily digested by enzymes of bacteria in different microbiomes (as free living or particle-attached microbes in intestinal, soil or marine ecosystems) as indicated by the carbohydrate-active enzyme database (*5*). The ocean has been compared to a “gigantic heterotrophic digester” (*6*) with marine heterotrophic bacteria as the “master recyclers” (*7*) and “gatekeepers” (*8*) in the carbon cycle. However, with light as an energy source, algae can catalyze net endergonic reactions that concentrate much more energy than is accessible to bacteria. Phytoplankton and macrophytes annually convert about 180 Gt of carbon dioxide into 123 Gt of glucose corresponding to 1.95×10^{21} Joule (1.950 Exajoule) of biochemical free energy. By comparison, nuclear power plants annually provide less than 10^{19} Joule (0.5%) of energy (2.738 TWh in 2023) (*9*).

Algae use some of the energy to synthesize organic molecules that control heterotrophic bacteria (*10*), including molecules that potentially affect their ability to release carbon dioxide. For example, diatoms, coccolithophores, and chlorophytes secrete broad acting antibiotics, such as benzoates, that suppress bacteria unless they have enzymes to detoxify these molecules (*11*). Both, micro- and macroalgae release dimethylsulfoniopropionate (DMSP) and other molecules that attract bacteria, which can provide nutrients, hormones, and vitamins

faster than diffusion (*11, 12*). Micro- and macroalgae are covered by a matrix of phylum-specific polysaccharides (e.g. fucoidan, ulvan, pectin, alginate) (*13*). These carboxylated glycans can sequester essential trace elements (*14*) at nanomolar concentrations (e.g. iron cations) via bi-pyramidal complexation by bidentate carboxyl group oxygens with one delocalized negative charge (*15, 16*). Since the metal cations that algae capture via their chelating matrices are also required by bacteria, e.g. as co-factors, competition for these nutrients limits bacterial growth in major parts of the ocean (e.g.(*17*)). Converging evidence suggests that either directly or indirectly, algae control the physiology of bacteria with organic molecules which determine heterotrophic processes that release carbon dioxide. However, evidence remains conflicting, whether or not secreted polysaccharides (glycans) perform this function.

Within the large pool of dissolved organic matter (*18*), algae-derived glycans contain substantial amounts of reduced carbon in the ocean. However, the structures, abundances, and relatively slow turnover rates of many of these glycans suggest that they are inferior substrates and therefore questionable agents to control microbiomes. Algal glycans are often sulfated. The glycosidic bond and sulfate ester bonds are both extremely stable and require million-fold hydrolysis rate enhancements to release the carbon energy (*19, 20*). Additional stability comes from the high intra- and intermolecular diversity of algal glycans, also termed glycan complexity. Given that most unique bonds in glycans require a unique enzyme, glycan complexity linearly increases enzyme diversity and proportionally decreases the quality of the glycan as a substrate (*21*). For example, the Verrucomicrobium *Lentimonas* sp. CC4 requires hundreds of enzymes to use structurally diverse fucoidans (*22*) that accumulate and sequester carbon in the ocean (*23, 24*). The synthesis of each additional enzyme increases the bacterial metabolic demand for nitrogen and phosphorous (*25*). When these nutrients are limited enzyme synthesis and in turn glycan consumption is affected. In contrast, algal photosynthetic glycan production can continue for some time under nutrient limitation, as evidenced by the increasing Redfield ratio of glycan-rich organic matter, especially during later phases of algal blooms (*26, 27*).

The resulting imbalance between synthesis and consumption produces a measurable excess of glycan carbon in the ocean. The carbon content in marine dissolved organic molecules (DOC) is on a similar scale as the carbon content in atmospheric carbon dioxide (*28, 29*). Algae-derived glycans account for a substantial part (5-30%) of the DOC pool (*30, 31*) and resist degradation for some time (*32*). According to compound-specific radiocarbon dating, these glycans account for ~20 µM of the ~100 µM dissolved organic carbon in the surface ocean and can evade remineralization for an average of one to three years (*32*). This stability was reproduced for weeks during bloom mesocosm experiments with the globally relevant phytoplankter *Emiliania huxleyi* (*27*). Likewise, glycan structural profiling with monoclonal antibodies has revealed a mixture of many structurally different, complex phytoplankton-derived glycans that persist or even accumulate for months in the presence of bacterioplankton (*23*). This persistence contrasts smaller algal metabolites that, without prior depolymerization, enter broadly conserved pathways shared among many taxonomically distinct bacteria. Consequently, these smaller molecules are consumed so rapidly that, unlike many glycans, their concentrations usually stay below one micromolar in both the ocean (*33*) and during laboratory experiments (*34*).

Conclusive environmental data show that overall algal glycan synthesis rates outcompete bacterial consumption, leading to an excess of diverse glycans (*23*). With this abundance, glycan carbon may not be a limiting resource and therefore not selective agents shaping the composition of microbiomes. Accordingly, only intracellular energy storage α- and β-glucans, such as glycogen and laminarin (*35*), were found to significantly enrich different bacterioplankton taxa during algal blooms (*36-38*). Whether algal glycans exert enough selection pressure to form a niche for specifically adapted bacteria and thereby shape or maybe even control the heterotrophic part of the carbon cycle remains unknown.

Results

To test whether glycans released by diatoms control the growth of bacteria, we aggregated five years of spring bloom datasets collected from the North Sea **(Fig. 1)** (*8, 37, 39-41*). Time

series metagenomes and metaproteomes repeatedly showed that diatoms enriched specific carbohydrate-active enzymes (CAZymes) within a group of bacterioplankton cells from the *Flavobacteriaceae* family that includes the *Polaribacter* genus (*8, 37, 41, 42*). These *Polaribacter* genomes contain a polysaccharide utilization locus (PUL) encoding putative sulfatases, homologs of glycoside hydrolase (GH) family 92, GH92 α-mannosidases and other enzymes of unknown function (*43, 44*). Diatoms represent the likely source of a corresponding mannan substrate for this PUL. This hypothesis has been supported by the finding of a sulfated, α-configured glucuronomannan in the benthic pennate model diatom *Phaeodactylum tricornutum* (*45, 46*). However, such a mannan remains unknown in planktonic, centric diatoms that constitute the majority of microalgal blooms (*47, 48*). Moreover, corresponding mannanases and mannosidases that are active on such a sulfated mannan remain unknown. Other studies independently found an association between *Polaribacter* spp. and diatoms based on 16S rRNA and 18S rRNA network analyses of phytoplankton-bacterioplankton blooms in the upwelling zones of the California coast (*49*) and the North Sea (*8*). This PUL has also been found in a fosmid clone library obtained from the North Atlantic (*50*), suggesting a putative mannan may be synthesized by planktonic diatoms and selects for bacterial genes beyond the North Sea and other marine regions.

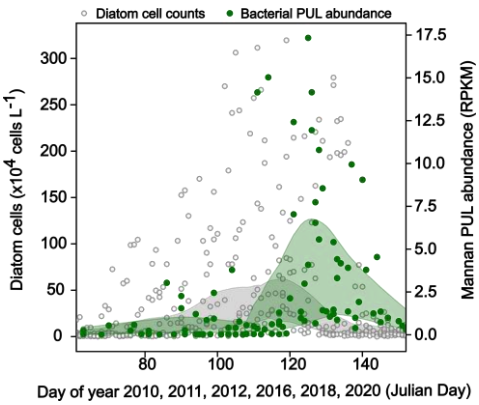

Figure 1: Diatom blooms enrich bacteria with mannan PULs suggesting α-mannan utilization. We aggregated phytoplankton bloom data from five years from the long-term ecological research station (LTER) on Helgoland. The data are fitted using locally weighted scatterplot smoothing and 95% confidence intervals (CI) were calculated using iterative bootstrapping (n=1,000). For better visibility upper and lower boundaries of confidence intervals are displayed as smooth curves. Gray area: Smoothed 95% CI for cell counts. Green area: Smoothed 95% CI for mannan PUL abundance. Gray dots: Diatom cell counts. Green dots: Mannan PUL abundance. The DNA sequence of the mannan PUL of *Polaribacter* sp.

Hel1_33_49 was mapped against metagenomes collected previously from the LTER, Helgoland Roads. PUL abundance over years was calculated in terms of Reads Per Kilobase per Million mapped reads (RPKM). For more information, see Materials and Methods.

Diatom secretes a sulfated mannan

We used the centric diatom *Thalassiosira weissflogii*, as a representative of diatoms frequently found during spring phytoplankton blooms in the North Sea, to find the possible target mannan. We used anionic exchange chromatography (AEX) to separate secreted, anionic glycans. Diatoms secrete a fucose containing sulfated polysaccharide (FCSP) (*23*). Here we show that the diatom secretes at least three anionic glycans, the FCSP, a glucuronomannan (*45, 46*) and a previously unknown homomannan. While the FCSP and the glucuronomannan eluted at lower salt concentration (0.5-1.2 M NaCl) and contained multiple different monosaccharides, a previously unknown homomannan was eluted at 2 M NaCl **(Fig. S1 A-C).** Acid hydrolysis followed by high performance AEX with pulsed amperometric detection (HPAEC-PAD) showed that the homomannan consisted of 95 mol % mannose. Additional ion chromatography revealed the mannan contains an almost equimolar ratio of sulfate to mannose **(Fig. S1 D)**. This relatively high content of negatively charged sulfate groups explains the strong binding of the mannan to the positively charged AEX column material. For its novelty, we concentrated on the characterization and potential degradation of this homomannan, hereafter the mannan.

During chromatography, concentration and dialysis the mannan remained soluble in seawater and in deionized water. We found a high solubility of up to 20 mg mL^{-1}, the highest concentration tested. At this concentration the algal polysaccharides agar, κ-carrageenan, alginate and pectin form gels in the presence of seawater concentrations of calcium and magnesium ions (*13*). The high solubility of the target mannan at environmental ion concentrations is significant because it verifies that the mannan is dissolved and may therefore bind to extracellular proteins from free-living, bacterioplankton cells, including the *Polaribacter* spp. that exclusively grow suspended but not on solid surfaces such as agar plates. Particle-associated bacteria may target other, insoluble glycans (*8*). We obtained between 15-20 mg of the mannan from 160 L of diatom culture (~100 µg L^{-1}). The diatom synthesized mannan

with a homogeneity, purity and quantity promising for structure determination by nuclear magnetic resonance spectroscopy (NMR).

A C6-sulfated α-1,3-mannan from a diatom

For configuration and connectivity determination of the mannan, we used one- and two-dimensional NMR **(Fig. 2 A, B)**. A detailed description is provided in the supplementary information. Briefly, the major component was α-1,3-D-mannopyranose with the majority of the C6 carbon de-shielded at 67.5 ppm showing 6-*O*-sulfation and confirming almost equimolar amounts of mannose and sulfate **(Fig. 2B, Supplementary Text)**. The spectra showed minor peaks that resembled xylose. For further verification we synthesized an oligosaccharide of the mannan and used it as reference structure for comparative NMR.

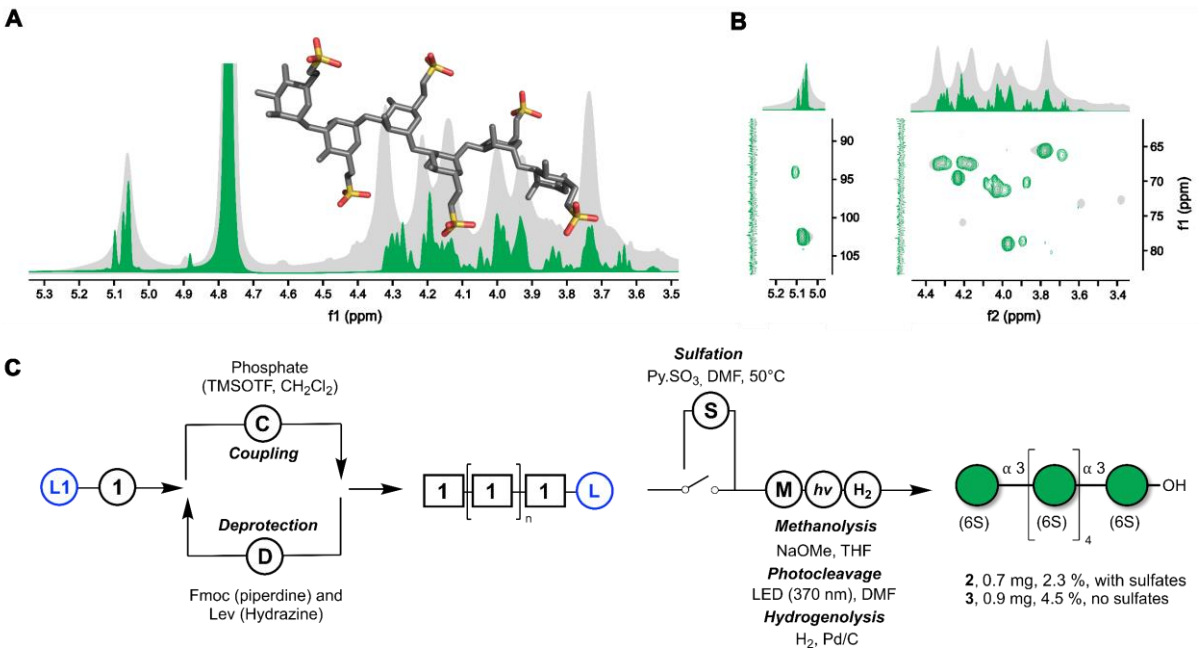

Figure 2: Diatoms synthesize a homo-mannan made of α-1,3-mannose-6-sulfate. In addition to chromatographic structure elucidation **(Fig. S1 B, D)** we used automated glycan assembly (AGA) to synthesize a mannan oligosaccharide of the NMR-hypothesized structure of the diatom mannan and compared the two spectra. (**A**) ^{1}H-NMR overlay of an automated glycan assembly derived, synthetic α-1,3-mannose-6-sulfate hexaoligosaccharide (green) and the mannan purified from *Thalassiosira weissflogii* culture supernatant (gray). (**B**) Shown is an overlay of ^{1}H-^{13}C HSQC spectra from the synthetic mannan hexamer (green) and the purified, diatom mannan (gray). NMR spectra at 700 MHz were collected at 20 °C. HSQC-TOCSY and ^{1}H-^{13}C HMBC can be found in supplementary data. (**C**) Scheme of chemical synthesis of mannan oligosaccharides. L1: free reducing end solid-phase linker (*51*). 1: Dibutyl 2-*O*-

benzoyl-4-*O*-benzyl-6-*O*-(9-fluorenylmethoxycarbonyl)-3-*O*-levulinoyl-1- phosphate-α-D-mannopyranoside.

We used automated glycan assembly to synthesize the reference mannan oligosaccharide. As building block we synthesized ethyl-2-*O*-benzoyl-4-*O*-benzyl-6-*O*-(9-fluorenylmethoxycarbonyl)-3-*O*-levulinoyl-1-thio-α-D-mannopyranoside. For automated assembly, the block was converted into a dibutyl phosphate donor **(1) (Fig. 2C, Supplementary Text)** to synthesize a hexa-α-1,3-mannose with one sulfate on each C6. Comparison of the NMR spectra of the natural and the synthetic mannan showed **(Fig. 2 A, B, Table S1)** deviations below 0.03 ppm in the proton and 0.16 ppm in the carbon dimensions. Hence, the structure is a C6-sulfated α-1,3-mannan. Next, we tested, whether the mannan can be used by the mannan PUL-containing *Polaribacter* species that were isolated from diatom blooms (*43, 44*) **(Fig. S2)**.

***Polaribacter* spp. consume diatom mannan**

To test if bacteria can utilize the mannan, we used the three *Polaribacter* strains Hel1_33_49, _78 and _96 that were isolated after a diatom-dominated spring bloom in the North Sea (*52*). Notably, these strains feature 100% identical 16S RNA genes and 98.5% genome-wide average nucleotide identity (ANI) (*53*) providing three biological replicates. The strains share the same gene architecture of and around the PUL, indicating a similar ability to degrade and metabolize the detected mannan. Accordingly, when the mannan was provided as a limited carbon source, the three strains grew **(Fig. S3-6, Table S2)**. As a negative control, we used *Polaribacter* sp. Hel1_88 (*52, 54*), whose genome lacks the mannan-PUL (*44*) and consequently this strain grew less on the mannan. Moreover, we found this bacterium, unlike the other *Polaribacter* strains, did not remove the mannan from the culture **(Fig. S4)**. In a previous metatranscriptome study we have shown *in situ* expression of this PUL by *Polaribacter* during a diatom-dominated North Sea spring bloom in the year 2020 (*37*). To confirm transcription and translation of enzymes capable of digesting the *T. weissflogii*

mannan, we used cell lysates of *Polaribacter* sp. Hel1_33_78 obtained from cells grown with or without the mannan, and we monitored the release of mannose over one week with enzymes from the different cultures **(Fig. S5,6)**. The enzymes in the cell lysates digested the mannan, confirming the aforementioned enzyme synthesis by *Polaribacter* during a North Sea algal bloom**.**

Enzymes specific for the diatom mannan

To verify enzyme activity and specificity, we used recombinant gene expression, enzymology and structural biology **(Fig. 3)**. The PUL comprises 23 genes **(Fig. S2)**, 21 of which encode putative enzymes. We cloned these genes from *Polaribacter* sp. Hel1_33_78 into vectors, transformed and expressed them in *Escherichia coli* BL21 (DE3) and conducted activity tests using the purified mannan, synthesized mannan and para-nitrophenyl-labeled substrates (PNP-substrates). The products were analyzed by fluorophore-assisted carbohydrate gel electrophoresis (FACE) and reducing sugar assays **(Table S3)**. To verify the findings, we obtained homologous enzymes from another marine flavobacterium, *Ochrovirga pacifica* S85*,* which was isolated from the Pacific Ocean (*55*) and has 69.8% ANI with the *Polaribacter* sp. Hel1_33_78 genome. *O. pacifica* has a distantly related version of the PUL (*56*) with 68.8% ANI to the mannan PUL of *Polaribacter* sp. Hel1_33_78. We found that four enzymes present in both PULs (*Polaribacter*: PbSulf1-GHx: WP_091953451.1, PbGH92_1: WP_091953473.1, PbSulf2: WP_231960077.1; *O. pacifica*: OpSulf1: WP_010136343.1, OpGHx: WP_010136376.1, GH92: WP_010136355.1, OpSulf2: WP_033194706.1) were active on the mannan comprising one unknown family GHx, one GH92 and two sulfatases. These enzymes hydrolyzed the mannan into mannose and sulfate. The remaining, 18 additional putative enzymes were cloned and tested but showed no activity on this mannan. Some of the other enzymes showed activity with PNP-substrates, and one enzyme was active on the glucuronomannan (not part of this study) that eluted before the here studied homomannan **(Table S3)**. Whenever possible, the validity of biochemical experiments was supported by X-

ray crystallography analysis and when the enzymes did not crystallize, we used *in silico* generated AlphaFold2 (*57*) structure models primarily to falsify the biochemical data.

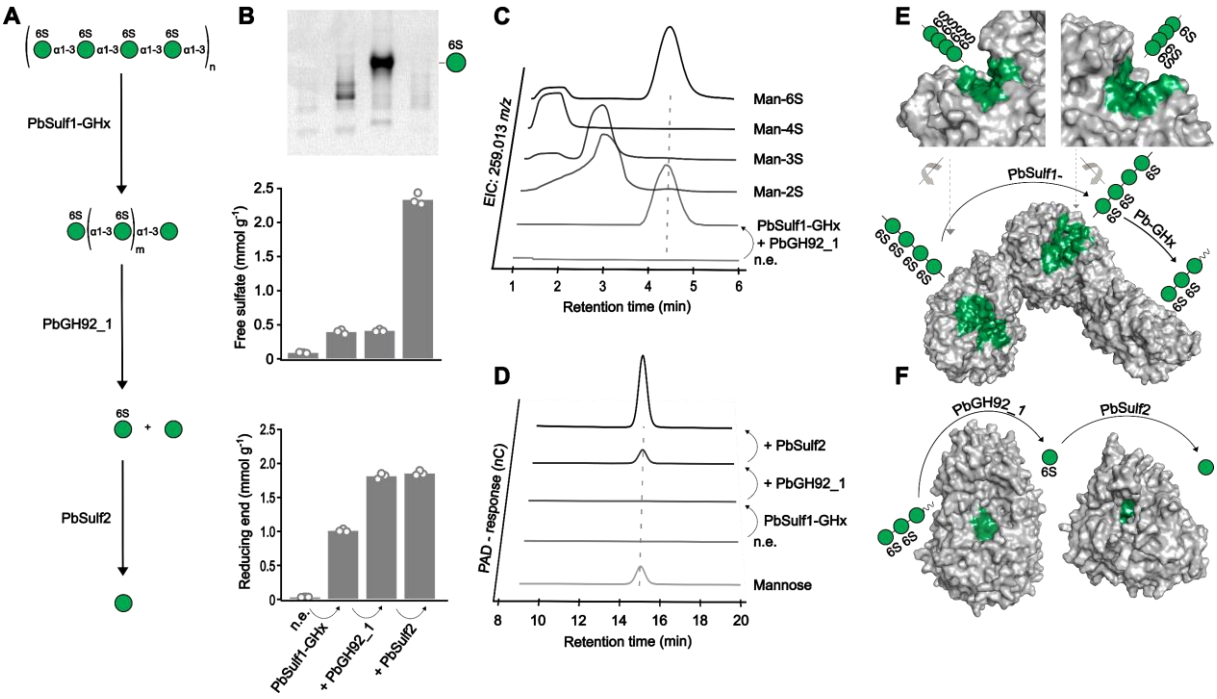

Figure 3: Four bacterial enzymes in three genes hydrolyzed the sulfated α-mannan from diatoms. (**A**). Suggested degradative pathway for sulfated α-mannan. (**B**) Enzymatic digestions of sulfated α-mannan via sequentially added PbSulf1-GHx, PbGH92_1 and PbSulf2. Top: Product separation by fluorophore-assisted carbohydrate electrophoresis using 2-aminoacridone as fluorophore. Middle: Free sulfate quantification. Bottom: Reducing end-assay. Bars represent mean of n=3 and circles display individual data points. n.e. = no enzyme. (**C**) Digestion of oligosaccharides produced by PbSulf1-GHx through PbGH92_1 were analysed using LC-MS. Extracted ion chromatograms at 259.013 *m/z* of the digestion compared with synthesized or commercially purchased mannose-sulfate standards. Man-2S: Mannose-2-Sulfate; Man-3S: Mannose-3-Sulfate; Man-4S: Mannose-4-Sulfate; Man-6S: Mannose-6-Sulfate. (**D**) Mannose release after a sequential digestion of sulfated α-mannan by PbSulf1-GHx, PbGH92_1 and PbSulf2 detected using HPAEC-PAD. (**E**-**F**) Structural model of enzymes involved in the degradative cascade were generated using AlphaFold2. Active site regions (green color) were identified using structural superimpositions with previously characterized enzymes. A simplified version of the degradative cascade is depicted according to the symbol nomenclature for glycans (*58*). (**E**) The PbSulf1-GHx tandem enzyme with the rotated active site region of the Sulfatase- and GHx-domain shown in top left and right, respectively. Grey arrows indicate the rotation axis of each domain towards the full-length protein (below). (**F**) Exo-acting PbGH92_1 and PbSulf2 have a pocket shape active site.

Mannan degradation is accomplished in four enzymatic steps. The first is catalyzed by the sulfatase domain and the second by the GHx domain in the multimodular enzyme PbSulf1-GHx that also contains a T9SS domain for extracellular secretion. The sulfatase domain belongs to the S1 family, subfamily 51 (*59*). It is the first described activity of this subfamily and

the first known sulfatase with this specificity. The GHx domain is distantly related to endo α-1,2 mannanases of the GH99 family and may therefore classify as a new family (*5*). Separating and visualizing fluorophore-labeled reaction products on FACE gels showed hydrolysis of the mannan by PbSulf1-GHx producing a ladder-like pattern of oligosaccharides typical for endo-acting enzymes **(Fig. 3B).** The enzyme released sulfate and oligosaccharides as shown by ion chromatography and reducing sugar assays **(Fig. 3B)**. Liquid chromatography mass spectrometry (LC-MS) showed that the tandem enzyme produced oligomers of sulfated hexoses with a degree of polymerization between three and seven **(Fig. S7)**. MS analyses showed that the oligosaccharides missed one sulfate group, e.g. a mannose tetra-oligosaccharide had only three sulfate groups indicating that both catalytic domains were active on the mannan.

We reproduced the results with the homologous enzymes from *O. pacifica,* where both catalytic domains are encoded by two separate genes. The enzymes OpSulf1 and OpGHx exhibit 53% and 36% amino acid identity to the *Polaribacter* spp. enzymes, respectively. The separated enzymes showed that the sulfatase was indeed necessary for the GHx to become active, suggesting that it requires a desulfated mannose for productive binding **(Fig. S8)**. The AlphaFold2 model of PbSulf1-GHx showed two appended catalytic domains with open, extended clefts **(Fig. 3E)** typical for endo-acting glycoside hydrolases (*60*) and sulfatases (*61*), corroborating the biochemical experiments. We obtained a crystal structure for the OpSulf1 at 1.49 Å resolution (**Fig. S9, Table S4**). The crystal structure confirmed an extended substrate binding cleft compatible with the elongated mannan chain. The conserved catalytic residues present in the center may remove one sulfate from the center of the bound mannan chain, which then becomes accessible to the GHx **(Fig. S9B, C)**. In conclusion, we identified and characterized two new enzyme activities, one C6-sulfate α-1,3-mannanase forming a new CAZy family and an endo C6-sulfate α-1,3-mannan sulfatase. These predicted outer membrane enzymes produce oligosaccharides of suitable size for import into the periplasm.

The third step was catalyzed by the periplasmic PbGH92_1, a mannosidase that removed C6-sulfated mannose from the oligosaccharides. Periplasmic localization of PbGH92_1 was

predicted by the Sec/SPI signal peptide (*62*). This enzyme belongs to the GH92 family (*63*). The GH92 family includes Ca^{2+}-dependent exo-acting α-1,2/3/4/6 mannosidases, but an enzyme acting on sulfated mannan remains unknown. Hydrolysis of mannan oligosaccharides into mannose-6-sulfate and a minor amount of mannose was shown by FACE, reducing sugar assay, HPAEC-PAD and MS **(Fig. 3B-D)**. The mannose-6-sulfate product was verified using LC-MS **(Fig. 3C)**. For this, we synthesized mannose-2/3/4-sulfate isomers **(Supplementary Text, Data S1, Fig. S10)**. The retention times revealed that only the mannose-6-sulfate aligned with the enzyme product peak and confirmed this isomer as the product of the PbGH92_1 **(Fig. S11)**. The AlphaFold2 model showed a pocket topology of size and shape typical for an exo-acting GH **(Fig. 3F)** binding one monomer in the -1 subsite (*60*). Conclusively, PbGH92_1 is a 6-sulfate α-1,3-mannosidase representing a new specificity within the GH92 family.

The fourth step was catalyzed by PbSulf2 that desulfates mannose-6-sulfate to yield mannose. A periplasmatic location was predicted by a Sec/SPII signal peptide. PbSulf2 is classified into sulfatase family S1, subfamily 11. Enzymes in this subfamily have been described to act on glucosamine-6-sulfate (*64*) and 6-sulfated porphyran oligosaccharides (*65*) but not on mannose-6-sulfate. PbSulf2 removes a sulfate group from mannose-6-sulfate as shown by appearance of the final product mannose in HPAEC-PAD measurements **(Fig. 3D)** and the disappearance of sulfated mannose in a complementary FACE experiment **(Fig. 3B).** The AlphaFold2 model aligned with the two previously described subfamily members (PDB ID Codes 5G2V / 7LJ2, rmsd: 0.613 Å / 0.845 Å) and showed a pocket topology typical for exo-acting sulfatases (*61*). Conclusively, PbSulf2 is a 6-sulfate α-1,3-mannose sulfatase representing a new activity within this enzyme family.

In summary, we elucidated a minimal enzymatic cascade consisting of four enzymes that achieve complete hydrolysis of the mannan into mannose and sulfate. The oligo- and monosaccharide structures produced by the enzymes confirmed the mannan structure solved with NMR.

Quantitative mannan synthesis and degradation

To quantify and verify the synthesis of the mannan by diatom cells and its consumption by *Polaribacter* spp., we used the enzymes to develop a quantitative assay. Hence, we used a combination of chromatography and enzymes for structure-specific quantification. The enzymes specifically produce mannose that provide a much stronger signal than the undigested polysaccharide with different quantitative approaches, e.g., reducing sugar assay or HPAEC-PAD **(Fig. S12A)**. Chromatographic separation and enrichment were crucial for the enzymes to digest the mannan**.** Without this purification step we found the enzymes remained inactive, potentially due to inhibitory interactions of sulfate groups from FCSP or other sulfated glycans with the enzymes in the mixture (*66*). After chromatographic separation, the biocatalytic assay detected up to 842 ± 62 µg L^{-1} in the diatom culture supernatant **(Fig. 4A).** The amount was positively correlated ($y = 3.97 \times 10^{-3}\ x - 2.94 \times 10^{-2}$, $P = 1 \times 10^{-23}$, $R^2 = 0.95$) with the number of diatom cells. Normalized for cell numbers, one *T. weissflogii* cell produced a net amount of 3.9 fmol mannan C **(Fig. 4B).** Substantially less mannan was present in diatom cells or particles **(Fig. S12B).** Notably, this new biocatalytic assay detects almost ten-fold more compared to our initial assessment based on the preparative mannan purification yield (~100 µg L^{-1}).

Next, we conducted growth experiments with *Polaribacter* sp. Hel1_33_49 and applied the analytic assay to quantify the consumption **(Fig. 4C)**. The bacteria grew to an OD_{600} of 0.2 when providing 0.1% (w/v) of the mannan as the limiting carbon source. Mannan concentration and bacterial abundance were negatively correlated ($y = -5.62\ x + 1.09$, $P = 1 \times 10^{-18}$, $R^2 = 0.96$) **(Fig. 4D)**. Conclusively, under nutrient-replete conditions the bacteria can remove the mannan within few days.

To test whether other diatoms also release this type of mannan, we adapted the biocatalytic assay into a qualitative version that rapidly identifies the structure of this mannan in different species. We tested *Thalassiosira pseudonana*, *Thalassiosira rotula* and *Chaetoceros affinis,*

members of genera that are common and of global ecological and biogeochemical relevance (*67*). We used AEX to enrich the mannan from each culture supernatant, applied the enzymes and analyzed the products using FACE **(Fig. 4E, F)**. For each diatom the first two enzymes (PbSulf1-GHx) produced the same set of oligosaccharides that we identified above as oligomers of C6-sulfated α-1,3-mannose missing one sulfate group. PbGH92_1 released mannose-6-sulfate, proving that the same mannan structure is produced by different diatoms. Secretion by different diatom species and detection of the mannan-specific PUL in the Pacific, North Atlantic and the North Sea indicated production by diatoms and adaptation of bacteria with specific enzymes around the globe. To test this hypothesis, we quantified the PUL and its association with diatoms in metagenomes from the planetary *Tara* Oceans dataset (*68*).

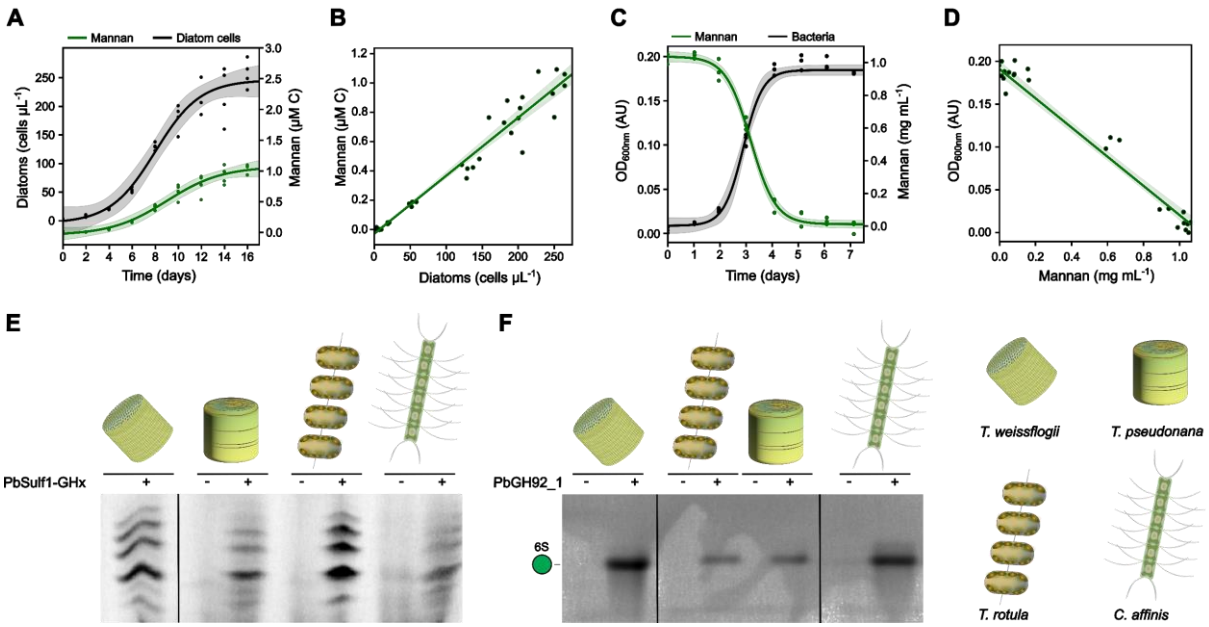

Figure 4: Synthesis of mannan by diatoms and consumption by bacteria quantified with the enzymatic cascade. (**A**)**.** Growth analysis of *Thalassiosira weissflogii* cultures using cell counts (black) and enzymatic quantification of sulfated α-mannan (green) in the anionic fraction of the culture supernatant. Data points were modeled using a logistic growth function employing the non-linear least squares method for fitting. n=4. (**B**) Linear regression analysis of diatom cell counts vs. mannan C production. The net production of mannan per cell was 3.9 fmol C cell^{-1} with an R^2=0.95. (**C**) *Polaribacter* sp. Hel1_33_49 grown with purified mannan for one week at 18 °C. The black line represents optical density measured at 600 nm. The green line shows the mannan consumption as detected via enzymatic quantification. Data points were modeled using a logistic growth function employing the non-linear least squares method for fitting. n=3. (**D**) Linear regression analysis of mannan concentration vs. optical density of the growth curve. (**E**-**F**) Mannan identification in anionic exudates purified from 0.5-5 M NaCl from AEX from *Thalassiosira weissflogii*, *Thalassiosira pseudonana*, *Thalassiosira rotula* and *Chaetoceros affinis*. Products were digested with PbSulf1-GHx (**E**) and PbGH92_1 (**F**) and

analyzed via fluorophore-assisted carbohydrate electrophoresis using 2-aminoacridone as fluorophore. Negative controls (-) contained heat inactivated enzyme.

Global utilization of diatom mannan by bacteria

To quantify the mannan PUL, we computed corresponding normalized read abundances (RPKM) within the *Tara* Oceans dataset. As negative and positive controls for glycan structure-based selection, we used bacterial PULs specific for known glycans from red, green and brown algal phyla. For example, diatoms occur as planktonic phytoplankton in all oceanic provinces, whereas the porphyran-producing red macroalgae *Porphyra* spp. is restricted to coastal areas, where it can grow attached to rocks. This confined range of the red algae may make the corresponding porphyran-PUL suitable as a negative control. Other preconditions for glycan controls were selected based on the precondition that the glycans are soluble and therefore accessible to planktonic bacteria, that the glycan structure has been verified by NMR and/or other methods and that the structure and function the PUL or a closely related variant has been empirically verified with biochemical experiments. As the negative control we used porphyran, a mixed link α-, β-galactan that is also sulfated on C6 and the corresponding PUL from the flavobacterium *Zobellia galactanivorans* Dsij^{T} (*69, 70*). As positive control, we used laminarin (chrysolaminarin), a β-glucan that is also produced by diatoms and the corresponding PUL from a metagenome-assembled genome (MAG C_MB344, accession: GCA_943788335) of a flavobacterial *Aurantivirga* species (*35-37*). Finally, we used ulvan, a sulfated rhamnogalacturonan produced by green macroalgal species such as *Ulva* spp. that can be both attached and planktonic moving between coastal and offshore regions (*71*) together with the characterized PUL (*72*)from the flavobacterium *Formosa agariphila* KMM 3901^{T} (*73, 74*).

Mannan PUL abundances ranged from 0.0025 to 0.41 RPKM in all of the 45 sampled sites including open and coastal ocean areas of the Atlantic, Pacific and Indian Ocean. The highest mannan PUL abundances were detected at upwelling sites (Benguela, Chile, Peru, California) where high nutrient concentrations induce diatom-dominated algal blooms (*47, 48*). The

laminarin PUL showed similar gene abundance levels at locations where we found the mannan PUL **(Fig. 5A, S13A)**. Consistently, we also found a linear correlation between the mannan PUL and the laminarin PUL ($y = 0.158\,x + 5.35 \times 10^{-3}$, $P = 4 \times 10^{-24}$, $R^2 = 0.91$). The porphyran PUL showed the lowest RPKM values of the tested glycans and was absent in the open ocean **(Fig. S13C).** The ulvan PUL showed overall similar abundance levels but at different locations compared to the mannan and laminarin PULs **(Fig. S13B)**. Consistently, the spatial presence and abundance of the mannan PUL was not correlated with the ulvan PUL ($P = 0.414$; $R^2 = 0.02$). The observed differences between the compared groups were significant across the dataset (Friedmann-Test: $P = 6 \times 10^{-21}$) supporting the algal phylum and glycan-specific selection for specifically adapted bacterial enzymes.

Metagenomics of bacterioplankton and eukaryotic 18S rRNA-based taxonomy revealed the enzymatic cascade to associate with centric diatoms. To further verify whether diatoms influence the abundance of the mannan PUL, we used previously reported total V9 read numbers as proxy for the abundance of centric diatoms (*48*). This approach was previously verified by showing the V9 reads to correlate with diatom algal cell counts (*75*). Linear regression analyses showed that the abundance of the mannan PUL correlated with the centric diatom read numbers ($y = 2.1 \times 10^{-7}\,x + 1.8 \times 10^{-3}$, $P = 3.1 \times 10^{-8}$, $R^2 = 0.82$) **(Fig. 5B)**. The laminarin PUL also significantly correlated with the centric diatom abundance ($y = 1.7 \times 10^{-6}\,x - 1.2 \times 10^{-2}$, $P = 2.5 \times 10^{-5}$, $R^2 = 0.64$) **(Fig. 5C)**. In contrast, we did not observe any correlation between the ulvan PUL and diatom cell abundances ($P = 0.94$; $R^2 = 0.00$), consistent with the synthesis of these different glycans by different algal taxa **(Fig. 5D)**. These data suggest that sulfated glycans are produced by diatoms and consumed by marine heterotrophic bacteria in substantial quantities on a global scale.

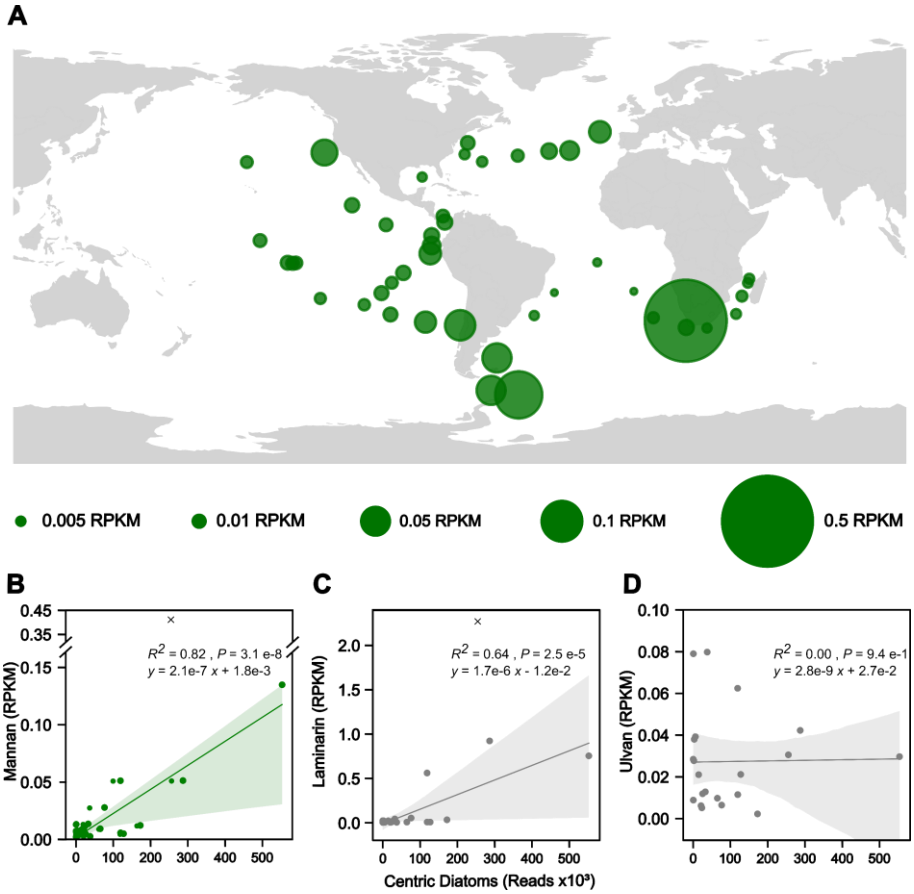

Figure 5: The mannan degrading enzymes are selected in the surface ocean around the globe. Global abundance of the mannan utilization locus from *Polaribacter* sp. Hel1_33_49 from *Tara* Oceans database. (**A**) The DNA sequence of the Mannan PUL was mapped against the raw metagenome reads of *Tara* Oceans surface water samples filtered at sizes ranging 0.2-3 µm across 45 different stations (*68*). Read abundances were calculated in terms of RPKM and normalized by length of the PUL and displayed as filled circles. Corresponding plots for the laminarin PUL from *Aurantivirga* MAG C_MB344 (*37*), the ulvan PUL from *Formosa agariphila* KMM 3901^T (*72*) and the porphyran PUL from *Zobellia galactanivorans* Dsij^T (*69*) can be found in SI. (**B**-**D**) Linear regression analyses of raw read abundance of centric diatom species in V9 rDNA metabarcoding dataset from *Tara* Oceans versus RPKM of different PULs across the same stations. Outliers where identified individually for each plot using the studentized residuals method with a threshold of three and excluded from the linear regression. Plots display the correlation analysis of centric diatoms vs (**B**) mannan PUL, (**C**) laminarin PUL and (**D**) ulvan PUL.

Discussion

Here, we describe the discovery of a sulfated mannan secreted by diatoms. Diatoms collectively account for at least 20% of the global primary production, with up to 70% in marine coastal upwelling areas and about 50% in marine temperate subpolar regions during spring and summer (*76*). We were able to isolate the mannan by chromatography from distinct diatom species. The homogeneity of the mannan is insofar remarkable, as homologous sulfated

glycans such as galactans (porphyran, λ-carrageenan) (*70*) and fucans (fucoidans) (e.g. (*77*)) are so heterogeneous that, to the best of our knowledge, direct structure determination with NMR, as achieved here for the mannan, has not been accomplished. This study shows that diatoms can synthesize a sulfated glycan of similar quality as the structure we synthesized via automated glycan assembly. This structural homogeneity produced by a diatom is important from a regulatory viewpoint when mannans are developed as drugs because their different structures are broadly bioactive. Anionic mannan oligosaccharides were tested as a potential therapeutic to treat Alzheimer Disease (*78*). Mannan oligosaccharides were shown to increase survival of the aquaculture shrimp *Litopaennaeus vannamei* by reducing the concentration of Vibrios and other pathogenic bacteria (*79*). We also discovered a corresponding enzymatic cascade of marine *Polaribacter* spp. that degrade the here introduced mannan. This cascade is encoded within a larger and well conserved PUL alongside additional mannan-related enzymes, which may act on other mannan structures, such as the glucuronomannan that we also identified in *T. weissflogii* **(Fig. S1B)**.

Our study demonstrates that distinct diatom glycans can be separated by AEX chromatography providing a tool for future structure function studies. The structures are consistent with different functions. An FCSP is highly complex providing stability against enzymatic invasion (*21*), a glucuronomannan with carboxyl groups can chelate and may therefore bind rare trace metal ions such as iron (*14*) and the simpler sulfated mannan may enrich for selected bacteria such as Polaribacter that can provide missing nutrients and metabolites to the diatom (*34*). The bacterial minimal cascade provides a biocatalytic assay for mannan quantification and to assess its role as potential carbon source and sink. The abundance of enzymes genes for degradation of mannan and laminarin was similar around the globe. Although there are currently no global measurements of this newly discovered mannan for previous lack of suitable assays, we know from measurements in different oceanic basins that laminarin has an annual production of 12 ± 8 Gt (*80*). Hence, based on similar enzyme abundances the mannan may be produced by marine diatoms and consumed by

bacteria in substantial quantities. Alternatively, it may be produced in smaller quantities and other factors are responsible for the mannan degrading genes being globally so abundant.

The structure of the mannan suggests positive and negative interactions with bacteria via protein binding. The C6-sulfation provides an extended linker that binds to positively charged amino acids on protein surfaces as shown for the structurally related red algal galactan porphyran (*69*). Owing to this extended linker the mannan is structurally similar to cationic exchange resins with sulfate groups that bind positively charged amino acids of proteins at physiological pH. It is therefore feasible that the negatively charged sulfate groups of the mannan form ionic bonds to and consequentially interfere with extracellular proteins of bacteria and other organisms. Such a hypothesized interference is supported by experiments in other fields including food and medical research where structurally related, sulfated glycans from algae are used or tested as surfactants, preservatives, as antibiofilm coatings and antimicrobials (*81, 82*). Bacteria around diatoms may be exposed to such interference and adapt with specific enzymes to evade surface active glycans as seen in the Polaribacter. This selection pressure may result in an abundance of mannanase genes similar to laminarin degrading enzymes that digest gigatons of laminarin produced by diatoms and other microalgae each year.

Members of *Polaribacter* are ubiquitous and often highly abundant in marine systems worldwide, as are diatoms (*54, 67, 83*). By digesting the mannan from diatoms the *Polaribacter* obtain energy and carbon, but they also remove potentially interfering sulfate groups from the mannan. This ability to depolymerize the mannan, during an algal bloom that is not limited in organic carbon, may explain why *Polaribacter* with these enzymes are so frequent. Of course, there are other strategies to evade surface active polyelectrolytes. For instance, SAR11 clade bacteria have surface properties that evade the surface active glycans that are used by marine animal filter feeders to trap and consume bacterioplankters (*84*). Low binding affinity of SAR11 to surface active glycans may, however, come at the cost of not being able to bind and therefore consume the energy and carbon these glycans provide. This hypothesis is consistent with SAR11 bacteria primarily using smaller carbon compounds as energy source (*85*). Such

a potential trade-off has been independently described for a closely related clade of several marine *Vibrio cyclitrophicus* strains showing signs of recent evolutionary speciation into two groups of binders and non-binders (*86*). The Vibrios with surface pili including the mannose sensitive hemagluttinin type surface pili (MSH) that are involved in host infection processes (*87*), can bind to and exploit surface bound glycans more effectively than the Vibrios without these genes. The Vibrios from the same clade but without the pili were less effective in resource exploitation but could also avoid being bound by the glycans (*88*). Binding of bacterial cells to surface active, adhesive glycans may remove those cells from the surface ocean by precipitation (*23*) akin to an antibody that removes pathogenic bacteria ether by coagulation or entanglement from the intestine (*89*). It is broadly accepted in microbiome research that glycans are prebiotic substrates for diverse bacteria and thereby structure microbiomes in diverse ecosystems (*90, 91*). However, polysaccharides can be beneficial for some (*92*) and at the same time detrimental for other bacteria (*93*) likely because they are broadly surface active. Uncovering these opposing roles of glycans in structuring microbiomes will require quantitative and structure specific glycan measurements. Opening our view from glycans as prebiotics to surface active molecules provides a new perspective on how glycans may structure microbiomes and regulate the carbon cycle.

Materials and Methods

Mannan PUL abundance in *TARA* Oceans dataset

Metagenome data of bacterioplankton during spring phytoplankton blooms was generated in previous studies from pre-filtered subsurface seawater (0.2-3 µm size fraction) sampled at the long-term ecological research site “Kabeltonne” (54° 11.3′ N, 7° 54.0′ E) at Helgoland Roads (North Sea) in the years 2010, 2011, 2012, 2016, 2018 and 2020 (*8, 37, 39-41*). For a global perspective, we used bacterioplankton metagenome data collected as part of *TARA* Oceans Expedition (*68*). Metagenomes from surface water samples collected across 45 different stations, filtered with sizes ranging from 0.2 to 3 µm, were used in the analysis. Mapping on

the metagenomes was performed using Bowtie2 (*94*) as part of SqueezeMeta v1.6.2 pipeline (Tamames 2019). PUL abundances in terms of reads per kilobase per million mapped reads (RPKM) were calculated using the formula: (metagenome reads mapped to the PUL*10^6)/(length of PUL in kbp × total reads in a metagenome). Differences between PUL abundances were statistically assessed using the Friedmann-Test. For correlation analyses with diatom abundance, we extracted the read numbers from 25 surface water samples (5-20 µm) from eukaryotic V9 metabarcoding data (*48*). V9 read numbers were used as proxy for absolute diatom abundance as explained before (*75*). V9 read abundances were correlated with the corresponding PUL abundances at the respective sites. Outliers were identified for each analysis using studentized residuals and excluded prior to linear regression analyses.

Diatom culture

The centric diatom *Thalassiosira weissflogii* was provided by André Scheffel (Max Planck Institute for Molecular Plant Physiology, Potsdam-Golm, Germany). *T. weissflogii* was cultured in 8x20 L batch cultures with non-axenic NEPCC medium (*95*) in 20 L Nalgene bottles at a constant temperature of 15 °C with a 16h/8 h light/dark cycle at an irradiance flux density of 140 μmol photons m^{-2} s^{-1}. Diatom growth was monitored by cell counting using a Neubauer counting chamber (Marienfeld, Königshofen, Germany). Cultures were inoculated using 1 L of preculture per 20 L bottle that were grown for ten days under the same conditions. Cells were separated from culture the supernatant using a continuous flow centrifuge (Thermo Fisher Scientific, Walthan, MA, USA) set at 150 mL min^{-1} and 6800 x g. The culture supernatant was filtered using a peristaltic pump through Whatman® glass microfiber filters (Grade GF/F, 0.70 µm) filters.

Preparative purification of mannan

For mannan purification, 160 L of *T. weissflogii* filtered culture supernatant were loaded onto a pre-equilibrated (50 mM Tris-HCl, 0.5 M NaCl, pH 7.5) 500 mL self-packed anion-exchange (AEX) column using ANX Sepharose 4 Fast Flow (High Sub) (Cytiva, Marlborough, MA, USA)

as column material. After loading, the column was washed with 1 L buffer solution (50 mM Tris-HCl, 1.35 M NaCl, pH 7.5). Mannan was subsequently eluted with 50 mM Tris-HCl with 2.5 M NaCl, pH 7.5. The purification was carried out at a flow rate of 50 mL min^{-1}. To remove salt, eluted fractions were repeatedly concentrated and diluted in MilliQ water (Merck KGaA, Darmstadt, Germany) over 30 kDa molecular weight cutoff membranes using an Amicon ultrafiltration stirred cell (Merck Millipore, Burlington, MA; USA) until the theoretical NaCl concentration was below 1 µM. The desalted sample was freeze-dried. For fractionation of the anionic high molecular weight DOM the same method was applied but instead of 1.35 and 2.5 M NaCl, 0.5 and 5 M NaCl were used. The dried compounds were then resuspended and loaded on a pre-packed 5 mL ANX column using ANX Sepharose 4 Fast Flow (High Sub) resin as column material (Cytiva). The column was equilibrated with 50 mM Tris-HCl pH 7.5 and for elution a stepwise elution with 0.5 M NaCl increments was applied up to 5 M NaCl. Per step, 15 mL of sample were collected. The samples were exhaustively dialyzed against MilliQ water (Merck) and freeze-dried prior to monosaccharide composition and sulfate analysis.

Glycan monosaccharide composition and sulfate content analyses

Desalted freeze-dried mannan obtained after anion exchange chromatography was dissolved in MilliQ water (Merck) to a concentration of 1 mg mL^{-1} and hydrolyzed using 1 M HCl at 100 °C for 24 h in pre-combusted glass vials. To remove HCl, samples were either vacuum centrifuged or diluted 1:1000 in MilliQ water (Merck) prior to further analyses. For monosaccharide measurements, we adapted a protocol for determination of neutral, amino- and acidic sugars using high performance anion exchange chromatography (HPAEC) described previously (*96*). In short, a Dionex ICS-5000+ system (Thermo Fisher Scientific) with pulsed amperometric detection (PAD) was equipped with a CarboPac PA10 analytical column (2 × 250 mm) and a CarboPac PA10 guard column (2 × 50 mm). System control and data acquisition were performed with Chromeleon v7.2 software (Thermo Fisher Scientific). Neutral and amino-monosaccharides were separated by an isocratic flow of 18 mM NaOH for 20 min, followed by

a gradient up to 200 mM sodium acetate over 10 min to separate acidic sugars. Monosaccharide standards were used to identify peaks by retention time and a standard mix ranging from 1–10 to 1000 µg L^{-1} was used to quantify the amount of monosaccharide (x-axis amount and y-axis peak area). The released sulfate from acid-hydrolyzed mannan was measured on a Metrohm 761 compact ion chromatograph (Metrohm, Herisau, Switzerland) with a Metrosep A Supp 5 column and suppressed conductivity detection with 0.5 M H_2SO_4. Ions were separated by an isocratic flow of carbonate buffer (3.2 mM Na_2CO_3 and 1 mM $NaHCO_3$) and the duration of a run was 20 min, with sulfate eluting at 16 min. Chromatograms were analyzed with the instrument's software MagIC Net version 3.2. All samples for monosaccharide and sulfate composition were prepared in triplicates.

Nuclear magnetic resonance and chemical synthesis of oligosaccharides

All chemicals used were reagent grade and used as supplied unless otherwise noted. A detailed description of the structural elucidation and glycan synthesis processes is provided in extended data. The automated syntheses were performed on a custom-built synthesizer developed at the Max Planck Institute of Colloids and Interfaces (Potsdam-Golm, Germany). Analytical thin-layer chromatography (TLC) was performed on Merck silica gel 60 F254 plates (0.25 mm). Compounds were visualized by UV irradiation or dipping the plate in a 5% H_2SO_4 ethanol solution. Flash column chromatography was carried out on an automated Grace flash chromatography system (Grace, Columbia, MD, USA). Analysis and purification by normal and reverse phase HPLC were performed using an Agilent 1200 series instrument (Agilent Technologies, Santa Clara, CA, USA). Products were lyophilized using a Christ Alpha 2-4 LD plus freeze dryer (Martin Christ GmbH, Osterode am Harz, Germany). ^{1}H-, ^{13}C- and HSQC-NMR spectra were recorded on a Varian 400-MR (400 MHz), Varian 600MR (600 MHz), or Bruker Biospin AVANCE700 (700 MHz) spectrometer (Varian, Palo Alto, CA, USA and Bruker Corp., Billerica, MA, USA). Signals were reported in terms of chemical shift [δ in parts per million (ppm)] relative to tetramethylsilane (TMS) or in D_2O using the solvent as the internal

standard in ^{1}H-NMR (D_2O: 4.79 ppm ^{1}H) as the internal standard. NMR data is presented as follows: Chemical shift, multiplicity (s = singlet, d = doublet, t = triplet, dd = doublet of doublet, m = multiplet and/or multiple resonances), coupling constant in Hertz (Hz), integration. All NMR signals were assigned on the basis of ^{1}H-NMR, ^{13}C-NMR, COSY, TOCSY and HSQC experiments. ‡Carbon assignments were extracted from HSQC experiments. High resolution mass spectra were obtained using a 6210 ESI-TOF mass spectrometer (Agilent) and a MALDI-TOF autoflex instrument (Bruker). MALDI and ESI mass spectra were run on IonSpec Ultima instruments (IonSpec, Lake Forest, CA, USA). The matrix used for MALDI-MS was 2,5-dihydroxy-benzoic acid (DHB).

Cloning of plasmids

Genes were cloned using the USER cloning or Gibson assembly methodologies (New England Biolabs, Ipswich, NE, USA) with genomic DNA from *Polaribacter* sp. Hel1_33_78 (strain provided by Jens Harder, Max Planck Institute for Marine Microbiology, Bremen, Germany). All primer pairs are provided in supplementary table S2. USER cloning constructs were cloned into a modified version of the pet28A vector promoter sequence as suggested by (*97*). Cloning of the modified vector backbone was achieved by ligating two PCR reactions of the empty pet28A Vector using the primer pairs pet28a_P1 and pet28a_P2 via the USER cloning method. Generally, all signal peptides were predicted using SignalP5.0 (*98*) and removed before cloning. PCR reactions were done with 30 cycles (denaturation: 95 °C, annealing: 55 °C, elongation: 72 °C) using 0.25 U of enzyme in a total reaction mix of 25 µl. DNA template was digested with DpnI and PCR products were purified using a commercially available PCR purification kit (Qiagen, Hilden, Germany). The USER reaction was carried out in a one pot reaction using 0.25 U of USER enzyme and a backbone:insert ratio of 0.015 pmol : 0.15 pmol in CutSmart buffer (New England Biolabs) in a total volume of 10 µL. The reaction was incubated at 37 °C for 20 minutes followed by 20 minutes at 25 °C and directly used for transformation into chemocompetent *E. coli* NEB5α (New England Biolabs). Plasmids from

transformed colonies were isolated using a commercial kit for plasmid preparation (Qiagen). All clones were verified by DNA sequencing. As the isolated *Polaribacter* spp. Hel1_33_49/78/96 does not grow on plates and were kept in cultivation since their initial isolation (*52*), we re-sequenced their genomes. The obtained constructs either aligned with the original or the re-sequenced genomic data of *Polaribacter* sp. Hel1_33_78. Re-sequenced genomic data of *Polaribacter* sp. Hel1_33_49 indicated highest purity of this strain. Owing to the genome identity of all strains (ANI > 98%), we used this strain for physiological experiments.

Recombinant enzyme expression and purification

Plasmids were transformed into *E. coli* BL21 (DE3) and expressed in 1 L lysogeny broth (LB) medium containing 50 µg mL^{-1} Kanamycin. The culture was grown at 37 °C under shaking until early exponential phase (OD_{600nm} 0.3-0.5). Recombinant expression was induced after cooling to 12 °C using 0.5 mM isopropyl-β-D-1-thiogalactopyranoside (IPTG) and further incubation at 12 °C for ~40 h. In the case of sulfatases, the formylglycine generating enzyme plasmid (Addgene plasmid repository, Watertown, MA, USA) (*99*) was co-transformed into the same expression host and expression was carried out as explained above except that cultures were additionally supplemented with 100 µg mL^{-1} Ampicillin and 0.02% L-arabinose was added right before cooling to 12 °C. Cells were collected by centrifugation (10,000 g, 4 °C, 45 min) and the cell pellets were stored at −20 °C. Cell lysis and purification were carried out as described previously (*100*) with the following exceptions: PbSulf1-GHx, PbGH92_1 and OpSulf1 were concentrated to 5 mg mL^{-1}, 4 mg mL^{-1} and 3.16 mg mL^{-1}, respectively. PbSulf2 was purified using a Talon column (Cytiva) without subsequent size exclusion and concentrated to 5 mg mL^{-1}. OpGHx was only purified with IMAC and concentrated to 0.5 mg mL^{-1}. For preliminary enzyme screening experiments one spatula of cell pellet were lyzed using BugBuster (Merck) according to manufacturer's instructions and cell debris was removed by centrifugation. Cell lysates were directly used for activity testing.

Enzyme activity

All digestions were carried out in 10 mM MOPS pH 7.5 and 500 mM NaCl with 0.1% (w/v) of mannan and enzymes were added in excess (0.01-0.1 mg mL^{-1}). In preliminary screening experiments 3.5% Sea Salts (Sigma Aldrich, Burlington, MA, USA) were used instead of NaCl and lysates were added at 10% (v/v). In screening experiments with para-nitrophenyl substrates, 1 mM per substrate were added. After overnight digestion, assays were heat inactivated at 95 °C for 5 min and centrifuged to remove precipitated proteins or cell debris. Supernatants were analyzed using fluorophore-assisted carbohydrate electrophoresis (FACE) with carbohydrates labeled with 2-aminoacridone as described in (*101*). Reducing-end measurements were carried out using PAHBAH as detection reagent as described previously (*102*). The release of sulfate and mannose from enzymatic reactions were measured using ion chromatography and HPAEC-PAD as described above, respectively. All enzymatic assays were carried out as technical replicates in triplicates unless otherwise stated.

Crystallization, data collection, structure solution, refinement and AlphaFold2

OpSulf1 solution of 3.16 mg/mL was used for initial crystallization attempts. Crystallization was performed in two drop 96-well crystallization plates in sitting drop format using commercial crystallization screens. Plates were incubated at 16 ºC. Start of the crystal formation was observed within 2-3 weeks. Diffraction quality crystals were obtained using 20% (w/v) polyethylene glycol 3,350, 200 mM potassium chloride. Crystals of the OpSulf1 required cryo-protection in crystallization solution supplemented with 20% glycerol prior to flash cooling in a liquid nitrogen at 100 K. Diffraction data was collected on DESY beamline P11. A total of 3600 images were collected (exposure: 0.1 s; oscillation: 0.1º). Measured reflections intensities were indexed, integrated and scaled using the autoproc pipeline available at the beamline facility. The OpSulf1 structure was solved to 1.9 Å using molecular replacement with the AlphaFold2 predicted model as reference in PHASER (*103*). For automatic model building,

BUCCANEER (*104*) was used. Refinement of the initial models was done in REFMAC5 (*105*) and further rounds of manual model building were carried out using COOT (*106*). Both models and structure factors for OpSulf_1 were deposited in the Protein Data Bank (PDB) with accession 9FVT. Corresponding data-processing and refinement statistics are summarized in Table S4. The structural comparison of OpSulf with homologs were performed using the PyMOL v.2.3.2 (Schrödinger, New York, NY, USA). Refinement data can be found in Table S4. For enzymes that did not crystallize we predicted using AlphaFold2 (*57*). All structures had predicted Local Distance Distance Test Values (pLDDT) of: PbSulf1-GHx_1 (pIDDT=91.2), PbGH92_1 (pIDDT=94.9), PbSulf2 (pIDDT=93.6) and OpGHx (pIDDT=94.2).

LC-MS of mannose-sulfate and mannan digests

Standards and digests were diluted in 90% UHPLC-grade and 10% (v/v) MilliQ water (Merck) for LC-MS measurements. 5 µL were injected to an Accucore-150-amide HILIC column (Thermo Fisher Scientific) held at 60 °C on a Thermo Fisher Vanquish Horizon UHPLC coupled to a Thermo Fisher Q-Exactive Plus MS. Mobile phases A and B consisted of 10 mM ammonium formate at pH 5 and UHPLC-grade acetonitrile, respectively. A gradient started after 1 min at 90% B and decreased from 90% to 40% B over 40 min at a flow rate of 0.4 mL min^{-1}. The column was equilibrated at 90% for 16 min at the end of each run. Mono- and oligosaccharides was detected in negative mode with the following MS conditions: spray voltage, 2.5 kV; sheath, auxiliary and sweep gas flow rates, 50, 13 and 3 respectively; capillary temperature, 260 °C; S-lens RF level, 60; auxiliary gas heater temperature, 425 °C; resolution, 70,000 at 200 *m/z*; scan range, 175 to 1,400 *m/z*, maximum IT, 100 ms; AGC target, 1E6. Mannose standards (synthetic or commercial) sulfated at various positions (2, 3, 4, 6) were also analyzed with LC-MS/MS with data-dependent acquisition. The *m/z* value of the $[M-H]^-$ ion (259.013) was provided in an inclusion list. MS/MS settings: resolution, 17,500; AGC target, 1E5; maximum IT, 50 ms; loop count, 3; isolation window, 0.4 *m/z*; normalized collision energy (NCE), 40. The intensity threshold was 1E5 and dynamic exclusion was applied for 10 s. A

721 targeted selected ion monitoring (tSIM) method was used for oligosaccharides yielded by
722 PbSulf1-GHx digestion of the mannan. Target ions identified in preliminary analyses were
723 provided as a timed inclusion list: 259.0131 *m/z*, 1-4 min; 421.0658 *m/z*, 8-10 min; 250.0078
724 *m/z*, 11-12 min; 377.0853 *m/z*, 6-11 min; 583.1192 *m/z*, 11-13 min; 331.0337 *m/z*, 12.5-14
725 min; 452.0390 *m/z*, 16-18 min; 573.0444 *m/z*, 19-21 min; 694.0494 *m/z*, 21-23 min; 543.0338
726 *m/z*, 23-25 min. SIM settings were as follows: resolution, 35,000 at 200 *m/z*; AGC target 5E4;
727 maximum IT, 100 ms; isolation window, 0.4 *m/z*. Thermo Fisher RAW files converted to mzML
728 format using the ProteoWizard 'msconvert' version 3.0.20239 with a 'peakPicking' filter (*107*).
729 'XCMS' (v3.16.1) was used to import data into R (*108*) and extract ion chromatograms (*109*).

730

731 **Bacterial growth**

732 Initial growth experiments with *Polaribacter* spp. Hel1_33_49/78/96 and Hel1_88 were carried
733 out in HaHa-medium supplemented with 0.1 mg mL^{-1} yeast extract and 2 mg mL^{-1} mannan
734 from either *T. weissflogii* or *C. affinis* (*110*). Growth was assessed using by measuring the
735 optical density at 600 nm. Additionally, monosaccharide compositions after acid hydrolysis of
736 the culture supernatant were analyzed as described above. *Polaribacter* sp. Hel1_33_78
737 grown on both substrates were harvested by centrifugation and the pellets were lysed using
738 BugBuster (Merck) according to manufacturer's protocol on glucose. Lysates were tested for
739 cross-reactivity on substrates from both, *T. weissflogii* and *C. affinis* mannan. Digests were
740 incubated overnight using 3.5% Sea Salts (Sigma), 10 mM MOPS pH 7.5 and 0.5 mg mL^{-1}
741 mannan and analyzed using carbohydrate-polyacrylamide gel electrophoresis (C-PAGE). C-
742 PAGE analysis was carried out as described in (*111*) except that stacking and resolving gels
743 were prepared with 10% and 25% acrylamide:bisacrylamide (19:1 v/v), respectively.
744 *Polaribacter* sp. Hel1_33_49 was grown in 3.5% Sea Salts (Sigma) supplemented with 0.03%
745 casaminoacids, 1x 7-vitamin and 1x trace elements solutions and 26 mg L^{-1} of ammonium
746 ferric citrate. Trace elements and 7-vitamin solutions were prepared as 1000x stocks as
747 described elsewhere (*110*). The mannan was used as limiting carbon source at a concentration

of 1 mg mL^{-1}. Growth was determined by measuring the absorbance at 600 nm. Growth curves were plotted with a logistic growth function using the non-linear least squares method. Substrate consumption was verified qualitatively using C-PAGE.

Enzymatic mannan quantification

Cultures of *Thalassiosira weissflogii* were grown in NEPCC medium as described above. Subsamples of 200 mL of culture were filtered using GF/F filters and loaded on equilibrated pre-packed 1 mL ANX columns using ANX Sepharose 4 Fast Flow (High Sub) (Cytiva). Columns were equilibrated with wash buffer containing 500 mM NaCl and 50 mM Tris-HCl pH7.5. After loading, the columns were washed with the same buffer buffer. Elution was done using a syringe containing 1.7 mL of elution buffer (5 M NaCl, 50 mM Tris-HCl pH 7.5). After syringe mounting, 200 µL of eluate were discarded and the following 1.5 mL were collected and desalted in 2 mL MilliQ water (Merck) using a desalting column according to manufacturer's instructions (Cytiva). Desalted samples were split in halves and dried using a vacuum centrifuge at 30 °C. One of each sample was digested in 20 µL using PbSulf1-GHx and PbGH92_1 as described above but with 3.5% Sea Salts (Sigma Aldrich). The second sample served as negative control. The digestion volume was 20 µL which were subsequently analyzed using PAHBAH. If necessary, PAHBAH reactions were diluted tenfold before measurement. For data analysis, negative control absorbances were subtracted from digestions. Results were compared with a standard curve containing defined amounts of mannan. The procedure recovery was determined to be at 80 ± 5% (n=3) compared to untreated mannan **(fig S7C)**.

Extraction of mannan from cellular biomass

After diatom cultivation the cell pellet was freeze-dried and sequentially extracted using MilliQ water (Merck), 0.4 M EDTA (pH 8) and 4 M NaOH with 0.1% NaBH4 (*23*). For 1 g of biomass

20 ml of sample were used. In each extraction step the sample was sonicated and centrifuged at 14.000 x g for 10 minutes. NaOH extracts were neutralized to pH 7.5 using HCl and diluted in MilliQ to < 500 mM NaCl. The mannan content in all extracts was determined as described above.

Detection of mannan from other diatoms

The diatom strains *Thalassiosira pseudonana*, *Chaetoceros affinis* and *Thalassiosira rotula* were cultivated as described above. 20 L of culture supernatant were concentrated after filtration using GF/F. For concentration, tangential ultrafiltration (Sartorius, Göttingen, Germany) with three cassettes of 30 kDa cutoff membranes (3051465901E–SG, Sartocon Slice PESU Cassettes, Sartorius Stedim) filters was applied resulting in 0.5 L concentrate. For dialysis, 20 L MilliQ water (Merck) were applied after sample loading. The dialyzed concentrate was loaded on a 500 mL anion exchange column as described above. The washing and elution buffers had 50 mM Tris-HCl NaCl pH 7.5 and contained 0.5 M and 5 M NaCl, respectively. The dialyzed and freeze-dried samples were used as substrates for enzymatic assays using PbSulf1-GHx_1 and PbGH92_1 as described above but instead of NaCl, 35 mg mL^{-1} Sea Salts (Sigma Aldrich) were used in the digestion. Digested samples were analyzed with FACE as described above.

Theoretical calculations

To convert the ocean net primary production into chemical energy we used the following assumptions with glucose containing -2.805×10^6 J mol^{-1} of combustible chemical energy. As this serves for comparison with net energy production in nuclear power plants, we did not convert this further to biologically available energy in the form of ATP. The following formula was used:

$$E_{Ocean,NPP} = \frac{N_C}{Mw_{C/Glucose}} \times \Delta H_{Glucose}$$

With N_C = 53 Pg C y^{-1} as the annual ocean carbon fixation through photosynthesis (*112*), $Mw_{C/Glucose}$ = 72 g $mol_{Glucose}^{-1}$ being the weight of carbon per mol glucose and $\Delta H_{Glucose}$ = - 2.805 × 10^6 J mol^{-1} being the enthalpy for glucose combustion.

References and Notes

1. C. B. Field, M. J. Behrenfeld, J. T. Randerson, P. Falkowski, Primary Production of the Biosphere: Integrating Terrestrial and Oceanic Components. *Science* **281**, 237 (1998).
2. J.-H. Hehemann *et al.*, Adaptive radiation by waves of gene transfer leads to fine-scale resource partitioning in marine microbes. *Nature Communications* **7**, 12860 (2016).
3. T. Dittmar *et al.*, Enigmatic persistence of dissolved organic matter in the ocean. *Nature Reviews Earth & Environment* **2**, 570-583 (2021).
4. R. A. Laine, A calculation of all possible oligosaccharide isomers both branched and linear yields 1.05 x 10^{12} structures for a reducing hexasaccharide: the Isomer Barrier to development of single-method saccharide sequencing or synthesis systems. *Glycobiology* **4**, 759-767 (1994).
5. E. Drula *et al.*, The carbohydrate-active enzyme database: functions and literature. *Nucleic Acids Res* **50**, D571-D577 (2022).
6. J. I. Hedges *et al.*, Evidence for non-selective preservation of organic matter in sinking marine particles. *Nature* **409**, 801-804 (2001).
7. A. Buchan, G. R. LeCleir, C. A. Gulvik, J. M. González, Master recyclers: features and functions of bacteria associated with phytoplankton blooms. *Nature Reviews Microbiology* **12**, 686-698 (2014).
8. F.-Q. Wang *et al.*, Particle-attached bacteria act as gatekeepers in the decomposition of complex phytoplankton polysaccharides. *Microbiome* **12**, (2024).
9. Energy Institute. Statistical Review of World Energy 2023 (2024). https://www.energyinst.org/statistical-review/. Accessed 2 July 2024
10. J. R. Seymour, S. A. Amin, J.-B. Raina, R. Stocker, Zooming in on the phycosphere: the ecological interface for phytoplankton–bacteria relationships. *Nature Microbiology* **2**, 17065 (2017).
11. N. Barak-Gavish *et al.*, Bacterial lifestyle switch in response to algal metabolites. *Elife* **12**, (2023).
12. E. E. Clerc *et al.*, Strong chemotaxis by marine bacteria towards polysaccharides is enhanced by the abundant organosulfur compound DMSP. *Nature Communications* **14**, 8080 (2023).
13. B. Kloareg, Y. Badis, J. M. Cock, G. Michel, Role and Evolution of the Extracellular Matrix in the Acquisition of Complex Multicellularity in Eukaryotes: A Macroalgal Perspective. *Genes*. 2021 (10.3390/genes12071059).
14. C. S. Hassler, V. Schoemann, C. M. Nichols, E. C. V. Butler, P. W. Boyd, Saccharides enhance iron bioavailability to Southern Ocean phytoplankton. *Proceedings of the National Academy of Sciences* **108**, 1076-1081 (2011).

15. D. A. Rees, Polysaccharide shapes and their interactions - some recent advances. **53**, 1-14 (1981).
16. C. Mohammed, L. Lalgee, M. Kistow, N. Jalsa, K. Ward, On the binding affinity and thermodynamics of sodium alginate-heavy metal ion interactions for efficient adsorption. *Carbohydrate Polymer Technologies and Applications* **3**, 100203 (2022).
17. S. Thiele, B. M. Fuchs, N. Ramaiah, R. Amann, Microbial community response during the iron fertilization experiment LOHAFEX. *Appl Environ Microbiol* **78**, 8803-8812 (2012).
18. D. A. Hansell, Recalcitrant dissolved organic carbon fractions. *Ann Rev Mar Sci* **5**, 421-445 (2013).
19. D. R. Edwards, D. C. Lohman, R. Wolfenden, Catalytic Proficiency: The Extreme Case of S–O Cleaving Sulfatases. *Journal of the American Chemical Society* **134**, 525-531 (2012).
20. R. Wolfenden, X. Lu, G. Young, Spontaneous Hydrolysis of Glycosides. *Journal of the American Chemical Society* **120**, 6814-6815 (1998).
21. M. Bligh, N. Nguyen, H. Buck-Wiese, S. Vidal-Melgosa, J. H. Hehemann, Structures and functions of algal glycans shape their capacity to sequester carbon in the ocean. *Curr Opin Chem Biol* **71**, 102204 (2022).
22. A. Sichert *et al.*, Verrucomicrobia use hundreds of enzymes to digest the algal polysaccharide fucoidan. *Nature Microbiology* **5**, 1026-1039 (2020).
23. S. Vidal-Melgosa *et al.*, Diatom fucan polysaccharide precipitates carbon during algal blooms. *Nat Commun* **12**, 1150 (2021).
24. H. Buck-Wiese *et al.*, Fucoid brown algae inject fucoidan carbon into the ocean. *Proc Natl Acad Sci U S A* **120**, e2210561119 (2023).
25. X. Yi *et al.*, Phosphate starvation stops bacteria digesting algal fucan that sequesters carbon. *bioRxiv*, 2024.2004.2007.588495 (2024).
26. I. Obernosterer, G. Herndl, Phytoplankton extracellular release and bacterial growth: Dependence on the inorganic N:P ratio. *Marine Ecology-progress Series - MAR ECOL-PROGR SER* **116**, 247-257 (1995).
27. A. Engel, S. Thoms, U. Riebesell, E. Rochelle-Newall, I. Zondervan, Polysaccharide aggregation as a potential sink of marine dissolved organic carbon. *Nature* **428**, 929-932 (2004).
28. M. McCarthy, J. Hedges, R. Benner, Major biochemical composition of dissolved high molecular weight organic matter in seawater. *Marine Chemistry* **55**, 281-297 (1996).
29. P. Friedlingstein *et al.*, Global Carbon Budget 2023. *Earth Syst. Sci. Data* **15**, 5301-5369 (2023).
30. L. I. Aluwihare, D. J. Repeta, A comparison of the chemical characteristics of oceanic DOM and extracellular DOM produced by marine algae. *Marine Ecology Progress Series* **186**, 105-117 (1999).
31. L. I. Aluwihare, D. J. Repeta, R. F. Chen, A major biopolymeric component to dissolved organic carbon in surface sea water. *Nature* **387**, 166-169 (1997).
32. L. I. Aluwihare, D. J. Repeta, S. Pantoja, C. G. Johnson, Two Chemically Distinct Pools of Organic Nitrogen Accumulate in the Ocean. *Science* **308**, 1007-1010 (2005).
33. K. Longnecker *et al.*, Seasonal and daily patterns in known dissolved metabolites in the northwestern Sargasso Sea. *Limnology and Oceanography* **69**, 449-466 (2024).
34. F. X. Ferrer-González *et al.*, Resource partitioning of phytoplankton metabolites that support bacterial heterotrophy. *The ISME Journal* **15**, 762-773 (2021).

35. S. Becker, A. Scheffel, M. F. Polz, J. H. Hehemann, Accurate quantification of laminarin in marine organic matter with enzymes from marine microbes. *Appl Environ Microb* **83**, e03389 (2017).
36. F. Unfried *et al.*, Adaptive mechanisms that provide competitive advantages to marine bacteroidetes during microalgal blooms. *The ISME Journal* **12**, (2018).
37. C. Sidhu *et al.*, Dissolved storage glycans shaped the community composition of abundant bacterioplankton clades during a North Sea spring phytoplankton bloom. *Microbiome* **11**, 77 (2023).
38. I. Beidler *et al.*, Alpha-glucans from bacterial necromass indicate an intra-population loop within the marine carbon cycle. *Nature Communications* **15**, 4048 (2024).
39. H. Teeling *et al.*, Recurring patterns in bacterioplankton dynamics during coastal spring algae blooms. *Elife* **5**, e11888 (2016).
40. G. Reintjes *et al.*, Short-term changes in polysaccharide utilization mechanisms of marine bacterioplankton during a spring phytoplankton bloom. *Environmental Microbiology* **22**, 1884-1900 (2020).
41. T. B. Francis *et al.*, Changing expression patterns of TonB-dependent transporters suggest shifts in polysaccharide consumption over the course of a spring phytoplankton bloom. *The ISME Journal* **15**, 2336-2350 (2021).
42. K. Krüger *et al.*, In marine Bacteroidetes the bulk of glycan degradation during algae blooms is mediated by few clades using a restricted set of genes. *The ISME Journal* **13**, 2800-2816 (2019).
43. P. Xing *et al.*, Niches of two polysaccharide-degrading Polaribacter isolates from the North Sea during a spring diatom bloom. *The ISME Journal* **9**, 1410-1422 (2015).
44. L. Kappelmann *et al.*, Polysaccharide utilization loci of North Sea Flavobacteriia as basis for using SusC/D-protein expression for predicting major phytoplankton glycans. *ISME J* **13**, 76-91 (2019).
45. C. Ford, E. Percival, 1299. Carbohydrates of Phaeodactylum tricornutum. Part II. A sulphated glucuronomannan. *Journal of the Chemical Society (Resumed)*, 7042-7046 (1965).
46. T. Le Costaouëc, C. Unamunzaga, L. Mantecon, W. Helbert, New structural insights into the cell-wall polysaccharide of the diatom Phaeodactylum tricornutum. *Algal Research* **26**, 172-179 (2017).
47. E. V. Armbrust, The life of diatoms in the world's oceans. *Nature* **459**, 185-192 (2009).
48. C. de Vargas *et al.*, Eukaryotic plankton diversity in the sunlit ocean. *Science* **348**, 1261605 (2015).
49. D. M. Needham, J. A. Fuhrman, Pronounced daily succession of phytoplankton, archaea and bacteria following a spring bloom. *Nature Microbiology* **1**, 16005 (2016).
50. P. R. Gómez-Pereira *et al.*, Genomic content of uncultured Bacteroidetes from contrasting oceanic provinces in the North Atlantic Ocean. *Environ Microbiol* **14**, 52-66 (2012).
51. K. Le Mai Hoang *et al.*, Traceless Photolabile Linker Expedites the Chemical Synthesis of Complex Oligosaccharides by Automated Glycan Assembly. *Journal of the American Chemical Society* **141**, 9079-9086 (2019).
52. R. L. Hahnke *et al.*, Dilution cultivation of marine heterotrophic bacteria abundant after a spring phytoplankton bloom in the North Sea. *Environmental Microbiology* **17**, 3515-3526 (2015).

53. M. Richter, R. Rosselló-Móra, F. Oliver Glöckner, J. Peplies, JSpeciesWS: a web server for prokaryotic species circumscription based on pairwise genome comparison. *Bioinformatics* **32**, 929-931 (2016).
54. B. Avcı, K. Krüger, B. M. Fuchs, H. Teeling, R. I. Amann, Polysaccharide niche partitioning of distinct Polaribacter clades during North Sea spring algal blooms. *The ISME Journal* **14**, 1369-1383 (2020).
55. Y. K. Kwon *et al.*, Ochrovirga pacifica gen. nov., sp. nov., a novel agar-lytic marine bacterium of the family Flavobacteriaceae isolated from a seaweed. *Curr Microbiol* **69**, 445-450 (2014).
56. C. S. Robb, A. A. Mystkowska, J. H. Hehemann, Crystal structure of a marine glycoside hydrolase family 99-related protein lacking catalytic machinery. *Protein Sci* **26**, 2445-2450 (2017).
57. J. Jumper *et al.*, Highly accurate protein structure prediction with AlphaFold. *Nature* **596**, 583-589 (2021).
58. A. Varki *et al.*, Symbol Nomenclature for Graphical Representations of Glycans. *Glycobiology* **25**, 1323-1324 (2015).
59. T. Barbeyron *et al.*, Matching the Diversity of Sulfated Biomolecules: Creation of a Classification Database for Sulfatases Reflecting Their Substrate Specificity. *PLOS ONE* **11**, e0164846 (2016).
60. G. Davies, B. Henrissat, Structures and mechanisms of glycosyl hydrolases. *Structure* **3**, 853-859 (1995).
61. A. G. Hettle *et al.*, The Molecular Basis of Polysaccharide Sulfatase Activity and a Nomenclature for Catalytic Subsites in this Class of Enzyme. *Structure* **26**, 747-758.e744 (2018).
62. F. Teufel *et al.*, SignalP 6.0 predicts all five types of signal peptides using protein language models. *Nature Biotechnology* **40**, 1023-1025 (2022).
63. Y. Zhu *et al.*, Mechanistic insights into a Ca^{2+}-dependent family of alpha-mannosidases in a human gut symbiont. *Nat Chem Biol* **6**, 125-132 (2010).
64. A. Cartmell *et al.*, How members of the human gut microbiota overcome the sulfation problem posed by glycosaminoglycans. *Proceedings of the National Academy of Sciences* **114**, 7037-7042 (2017).
65. C. S. Robb *et al.*, Metabolism of a hybrid algal galactan by members of the human gut microbiome. *Nature Chemical Biology* **18**, 501-510 (2022).
66. K. T. Kim, L. E. Rioux, S. L. Turgeon, Alpha-amylase and alpha-glucosidase inhibition is differentially modulated by fucoidan obtained from Fucus vesiculosus and Ascophyllum nodosum. *Phytochemistry* **98**, 27-33 (2014).
67. S. Malviya *et al.*, Insights into global diatom distribution and diversity in the world's ocean. *Proceedings of the National Academy of Sciences* **113**, E1516-E1525 (2016).
68. Tara Oceans Consortium, P. Tara Oceans Expedition. Participants (2017): Registry of all samples from the Tara Oceans Expedition (2009-2013) [dataset publication series]. PANGAEA, https://doi.org/10.1594/PANGAEA.875582.
69. J.-H. Hehemann *et al.*, Biochemical and Structural Characterization of the Complex Agarolytic Enzyme System from the Marine Bacterium Zobellia galactanivorans*. *Journal of Biological Chemistry* **287**, 30571-30584 (2012).
70. G. Correc, J. H. Hehemann, M. Czjzek, W. Helbert, Structural analysis of the degradation products of porphyran digested by Zobellia galactanivorans beta-porphyranase A. *Carbohyd Polym* **83**, 277-283 (2011).
71. V. Smetacek, A. Zingone, Green and golden seaweed tides on the rise. *Nature* **504**, 84-88 (2013).

72. L. Reisky *et al.*, A marine bacterial enzymatic cascade degrades the algal polysaccharide ulvan. *Nat Chem Biol* **15**, 803-812 (2019).
73. O. I. Nedashkovskaya *et al.*, Formosa agariphila sp. nov., a budding bacterium of the family Flavobacteriaceae isolated from marine environments, and emended description of the genus Formosa. *Int J Syst Evol Microbiol* **56**, 161-167 (2006).
74. A. J. Mann *et al.*, The genome of the alga-associated marine flavobacterium Formosa agariphila KMM 3901T reveals a broad potential for degradation of algal polysaccharides. *Appl Environ Microbiol* **79**, 6813-6822 (2013).
75. C. Vargas *et al.* (2015). First Tara Oceans V9 rDNA metabarcoding dataset (2015) http://taraoceans.sb-roscoff.fr/EukDiv/. Accessed 2 July 2024.
76. J. Uitz, H. Claustre, B. Gentili, D. Stramski, Phytoplankton class-specific primary production in the world's oceans: Seasonal and interannual variability from satellite observations. *Global Biogeochemical Cycles* **24**, (2010).
77. A. Sichert *et al.*, Ion-exchange purification and structural characterization of five sulfated fucoidans from brown algae. *Glycobiology* **31**, 352-357 (2021).
78. S. Xiao *et al.*, A 36-week multicenter, randomized, double-blind, placebo-controlled, parallel-group, phase 3 clinical trial of sodium oligomannate for mild-to-moderate Alzheimer's dementia. *Alzheimer's Research & Therapy* **13**, 62 (2021).
79. O. Gainza, J. Romero, Effect of mannan oligosaccharides on the microbiota and productivity parameters of Litopenaeus vannamei shrimp under intensive cultivation in Ecuador. *Scientific Reports* **10**, 2719 (2020).
80. S. Becker *et al.*, Laminarin is a major molecule in the marine carbon cycle. *Proc Natl Acad Sci U S A* **117**, 6599-6607 (2020).
81. H. Ruan *et al.*, Polysaccharide-based antibacterial coating technologies. *Acta Biomaterialia* **168**, 42-77 (2023).
82. J. d. J. Paniagua-Michel, J. Olmos-Soto, E. R. Morales-Guerrero, in *Advances in Food and Nutrition Research,* S.-K. Kim, Ed. (Academic Press, 2014), vol. 73, pp. 221-257.
83. J. T. Staley, J. J. Gosink, Poles apart: biodiversity and biogeography of sea ice bacteria. *Annu Rev Microbiol* **53**, 189-215 (1999).
84. A. Dadon-Pilosof *et al.*, Surface properties of SAR11 bacteria facilitate grazing avoidance. *Nature Microbiology* **2**, 1608-1615 (2017).
85. J. Sun *et al.*, One carbon metabolism in SAR11 pelagic marine bacteria. *PLoS One* **6**, e23973 (2011).
86. B. J. Shapiro *et al.*, Population genomics of early events in the ecological differentiation of bacteria. *Science* **336**, 48-51 (2012).
87. A. S. Utada *et al.*, Vibrio cholerae use pili and flagella synergistically to effect motility switching and conditional surface attachment. *Nature Communications* **5**, 4913 (2014).
88. Y. Yawata *et al.*, Competition-dispersal tradeoff ecologically differentiates recently speciated marine bacterioplankton populations. *Proc Natl Acad Sci U S A* **111**, 5622-5627 (2014).
89. K. Moor *et al.*, High-avidity IgA protects the intestine by enchaining growing bacteria. *Nature* **544**, 498-502 (2017).
90. J. M. Grondin, K. Tamura, G. Dejean, D. W. Abbott, H. Brumer, Polysaccharide utilization loci: fueling microbial communities. *J Bacteriol* **199**, e00860-00816 (2017).

91. N. M. Koropatkin, E. A. Cameron, E. C. Martens, How glycan metabolism shapes the human gut microbiota. *Nature Reviews Microbiology* **10**, 323-335 (2012).
92. R. B. Cassie *et al.*, Carbohydrate-active enzymes from Akkermansia muciniphila breakdown mucin O-glycans to completion. *bioRxiv*, 2024.2003.2027.586211 (2024).
93. K. M. Wheeler *et al.*, Mucin glycans attenuate the virulence of Pseudomonas aeruginosa in infection. *Nature Microbiology* **4**, 2146-2154 (2019).
94. B. Langmead, S. L. Salzberg, Fast gapped-read alignment with Bowtie 2. *Nature Methods* **9**, 357-359 (2012).
95. P. J. Harrison, R. E. Waters, F. J. R. Taylor, A broad spectrum artificial sea water medium for coastal and open ocean phytoplankton. *Journal of Phycology* **16**, 28-35 (1980).
96. A. Engel, N. Händel, A novel protocol for determining the concentration and composition of sugars in particulate and in high molecular weight dissolved organic matter (HMW-DOM) in seawater. *Marine Chemistry* **127**, 180-191 (2011).
97. P. J. Shilling *et al.*, Improved designs for pET expression plasmids increase protein production yield in Escherichia coli. *Communications Biology* **3**, 214 (2020).
98. J. J. Almagro Armenteros *et al.*, SignalP 5.0 improves signal peptide predictions using deep neural networks. *Nature Biotechnology* **37**, 420-423 (2019).
99. I. S. Carrico, B. L. Carlson, C. R. Bertozzi, Introducing genetically encoded aldehydes into proteins. *Nat Chem Biol* **3**, 321-322 (2007).
100. V. Solanki *et al.*, Glycoside hydrolase from the GH76 family indicates that marine Salegentibacter sp. Hel_I_6 consumes alpha-mannan from fungi. *ISME J* **16**, 1818-1830 (2022).
101. J. H. Hehemann *et al.*, Transfer of carbohydrate-active enzymes from marine bacteria to Japanese gut microbiota. *Nature* **464**, 908-912 (2010).
102. S. Becker, J.-H. Hehemann, Laminarin Quantification in Microalgae with Enzymes from Marine Microbes. *Bio-protocol* **8**, e2666 (2018).
103. A. J. McCoy *et al.*, Phaser crystallographic software. *J Appl Crystallogr* **40**, 658-674 (2007).
104. K. Cowtan, The Buccaneer software for automated model building. 1. Tracing protein chains. *Acta Crystallogr D Biol Crystallogr* **62**, 1002-1011 (2006).
105. G. N. Murshudov *et al.*, REFMAC5 for the refinement of macromolecular crystal structures. *Acta Crystallogr D Biol Crystallogr* **67**, 355-367 (2011).
106. P. Emsley, B. Lohkamp, W. G. Scott, K. Cowtan, Features and development of Coot. *Acta Crystallogr D Biol Crystallogr* **66**, 486-501 (2010).
107. M. C. Chambers *et al.*, A cross-platform toolkit for mass spectrometry and proteomics. *Nature Biotechnology* **30**, 918-920 (2012).
108. R. C. Team, R: A Language and Environment for Statistical Computing. (2021).
109. C. A. Smith, E. J. Want, G. O'Maille, R. Abagyan, G. Siuzdak, XCMS: processing mass spectrometry data for metabolite profiling using nonlinear peak alignment, matching, and identification. *Anal Chem* **78**, 779-787 (2006).
110. R. L. Hahnke, J. Harder, Phylogenetic diversity of Flavobacteria isolated from the North Sea on solid media. *Syst Appl Microbiol* **36**, 497-504 (2013).
111. M. Robb, J. K. Hobbs, A. B. Boraston, Separation and Visualization of Glycans by Fluorophore-Assisted Carbohydrate Electrophoresis. *Methods Mol Biol* **1588**, 215-221 (2017).

112. K. S. Johnson, M. B. Bif, Constraint on net primary productivity of the global ocean by Argo oxygen measurements. *Nature Geoscience* **14**, 769-774 (2021).
113. Y. Zhu, M. Delbianco, P. H. Seeberger, Automated Assembly of Starch and Glycogen Polysaccharides. *Journal of the American Chemical Society* **143**, 9758-9768 (2021).
114. O. T. Tuck, E. T. Sletten, J. Danglad-Flores, P. H. Seeberger, Towards a Systematic Understanding of the Influence of Temperature on Glycosylation Reactions. *Angewandte Chemie International Edition* **61**, e202115433 (2022).
115. J. M. A. van Hengst *et al.*, Mapping the effect of configuration and protecting group pattern on glycosyl acceptor reactivity. *Chemical Science* **14**, 1532-1542 (2023).
116. O. J. Plante, R. B. Andrade, P. H. Seeberger, Synthesis and Use of Glycosyl Phosphates as Glycosyl Donors. *Organic Letters* **1**, 211-214 (1999).
117. C. J. S.-J. Crawford, M.; Luong, P.; Vidal-Melgosa, S.; Hehemann, J.-H.; Seeberger, P. H., Automated Synthesis of Fucoidan Enables Molecular Investigations in Marine Glycobiology. *ChemRxiv*, (2024).
118. B. Domon, C. E. Costello, A systematic nomenclature for carbohydrate fragmentations in FAB-MS/MS spectra of glycoconjugates. *Glycoconjugate Journal* **5**, 397-409 (1988).

Acknowledgements:

We thank Manual Liebeke for access to LC-MS devices. We also thank C. Eschen, P. Subramanya, P. Schoppmeier for large-scale cultivation of *Thalassiosira weissflogii* and K. Imhoff for advice and support during sulfate quantification and T. Trautmann, A. Bolte and K. Föll for technical support. We thank Hagen Buck-Wiese for help with the LC-MS analysis.

Funding: J.H.H. was funded by the German Research Foundation through the Heisenberg program Grant (HE 7217/5-1). The work was supported by the European Research Council, ERC grant, C-Quest, (Grant 101044738) to J.H.H. This study was supported by the German Federal Ministry of Education and Research (BMBF) in the frame of the BaMS-BALI project (031B0915D1/2) and the German Research Foundation (DFG) for the Research Unit FOR 2406 “Proteogenomics of Marine Polysaccharide Utilization” (POMPU) by Grants to J.H.H. (HE 7217/2-3), T.S. (SCHW 595/10-3) and H.T (TE 813/2-3). C.J.C. was funded by MSCA grant: MARINEGLYCAN (101029842). Generous financial support of the Max-Planck Society is gratefully acknowledged (P.H.S., J.H.H, C.J.C., R.K.S.).

Author contributions: J.K. and J.H.H. planned the experiments with support by T.S. J.K. cloned and expressed the genes, conducted all activity assays, purified the glycans and cultured marine diatoms. P.H.S., C.J.C. and R.K.S. synthesized the oligosaccharide and mannose-sulfate standards and conducted all NMR experiments. V.S. provided structural models and refined the crystal structure. H.T., C.S., J.K. and J.H.H. conducted metagenome analyses. L.R. purified the proteins, set up crystallization experiments and edited the manuscript. M.B. conducted LC-MS experiments. J.K. and J.H.H. wrote the manuscript with input from all authors. **Competing interests**: All authors declare that they have no competing interests. **Data and materials availability:** All data are available in the manuscript or the supplementary materials.

List of Supplementary Materials:

Supplementary Text

Figs. S1 to S31

Scheme S1

Table S1 to S6

Chemical Synthesis

References (*113-117*)